Inorganic Chemistry

Article

pubs.acs.org/IC

Biscyclometalated Ruthenium Complexes Bridged by 3,3′,5,5′-Tetrakis(*N*-methylbenzimidazol-2-yl)biphenyl: Synthesis and Spectroscopic and Electronic Coupling Studies

Jiang-Yang Shao, Wen-Wen Yang, Jiannian Yao, and Yu-Wu Zhong*

Beijing National Laboratory for Molecular Sciences, CAS Key Laboratory of Photochemistry, Institute of Chemistry, Chinese Academy of Sciences, Beijing 100190, People's Republic of China

Supporting Information

ABSTRACT: A series of biscyclometalated ruthenium complexes bridged by the title ligand were prepared by either an oxidative dimerization of corresponding monometallic complexes or treatment of the bridging ligand with $Ru(L)Cl_3$ (L = capping ligand). The electronic properties of these complexes were examined by electrochemical and spectroscopic analysis and DFT/TDDFT calculations. The degree of metal−metal electronic coupling of these complexes was estimated on the basis of intervalence charge-transfer transition analysis of corresponding mixed-valent complexes. These studies indicated that the electronic coupling was strongly dependent on the electronic nature of the terminal ligands. A hole-transfer superexchange mechanism was used to understand the underlying electron-transfer processes.

INTRODUCTION

Since disclosure of the Creutz−Taube ion,[1] {[$Ru(NH_3)_5$](pyrazine)[$Ru(NH_3)_5$]$^{5+}$}, tremendous efforts have been devoted to the studies of dimetallic mixed-valent (MV) complexes.[2] The degree of electronic coupling between individual metal centers depends on a number of key factors, including the distance between metal centers, the coordination environments of metal components, and the ability of the bridging ligand to delocalize the electronic charge.[3] According to the degree of electronic coupling (from weak to moderate and very strong), MV systems can be distinguished as Robin and Day class I−III categories.[4] MV complexes can be taken as simple model systems for studying electron-transfer processes between organic bridge-connected electronic donors and acceptors. These studies provide useful information relevant to molecular electronics and many naturally occurring photoinduced electron/energy-transfer processes.[3]

One of the interesting redox centers for MV systems is a ruthenium metal supported by a covalent bond with carbon,[5] nitrogen,[6] or oxygen anions[7] (so-called cyclometalated ruthenium).[8] As a result of the electron-rich nature of these anionic ligands, corresponding $Ru^{II/III}$ processes of these complexes take place at a much lower potential than those surrounded by all dative bonds. However, the exact redox potential of the $Ru^{II/III}$ process is dependent on the auxiliary ligands. For instance, cyclometalated ruthenium complexes with pyridine,[9] triazole,[10] or benzimidazole[11] ligands exhibit distinctly different metal-based redox events. It has been reported that MV systems with cyclometalated ruthenium displayed enhanced electronic coupling versus their noncyclometalated counterparts.[12] However, the degree of metal−metal electronic coupling in MV systems with cyclometalated ruthenium is also strongly dependent on the auxiliary ligands. The use of pyridine,[13] triazole,[14] dimethylamino,[15] or diphenylphosphine[16] groups as auxiliary ligands resulted in different degrees of electron delocalization in these complexes. We report in this article the synthesis and electronic property studies of a series biscyclometalated ruthenium complexes bridged by 3,3′,5,5′-tetrakis(*N*-methylbenzimidazol-2-yl)biphenyl, where *N*-methylbenzimidazole moieties are used as the auxiliary ligands to support metal−metal electronic communication through the biphenyl backbone. It should be noted that MV systems with benzimidazole-containing noncyclometalated ruthenium centers have been reported previously.[17] However, biscyclometalated ruthenium complexes supported by benzimidazole ligands have not been documented, to the best of our knowledge.

RESULTS AND DISCUSSION

Synthesis. We have studied three diruthenium complexes ($\mathbf{2}^{2+}$, $\mathbf{4}^{2+}$, and $\mathbf{7}^{2+}$; Scheme 1) bridged by the title ligand in this paper. Experimental details and characterization data for synthesis of these complexes are provided in the Experimental Section. Complex $\mathbf{2}^{2+}$ was obtained via the oxidative coupling of the monometallic complex $\mathbf{1}^{+}$ in the presence of $AgBF_4$.[12] However, attempts to prepare complex $\mathbf{4}^{2+}$ capped by the electron-donating ligands bis(*N*-methylbenzimidazolyl)pyridine (Mebip) from $\mathbf{3}^{+}$ failed under the same reaction conditions. The only isolated product is the one-electron-oxidized complex $\mathbf{3}^{2+}$, which has been reported in a previous paper by us.[11] The significantly lower oxidation potential of $\mathbf{3}^{+}$ compared to $\mathbf{1}^{+}$ may account for this difference (+0.26 vs +0.48 V vs Ag/AgCl).[11] We then turned our attention to the bridging

Received: January 10, 2012
Published: March 9, 2012

   dx.doi.org/10.1021/ic300054j | *Inorg. Chem.* 2012, 51, 4343−4351

Scheme 1. Synthesis of the Compounds Studied

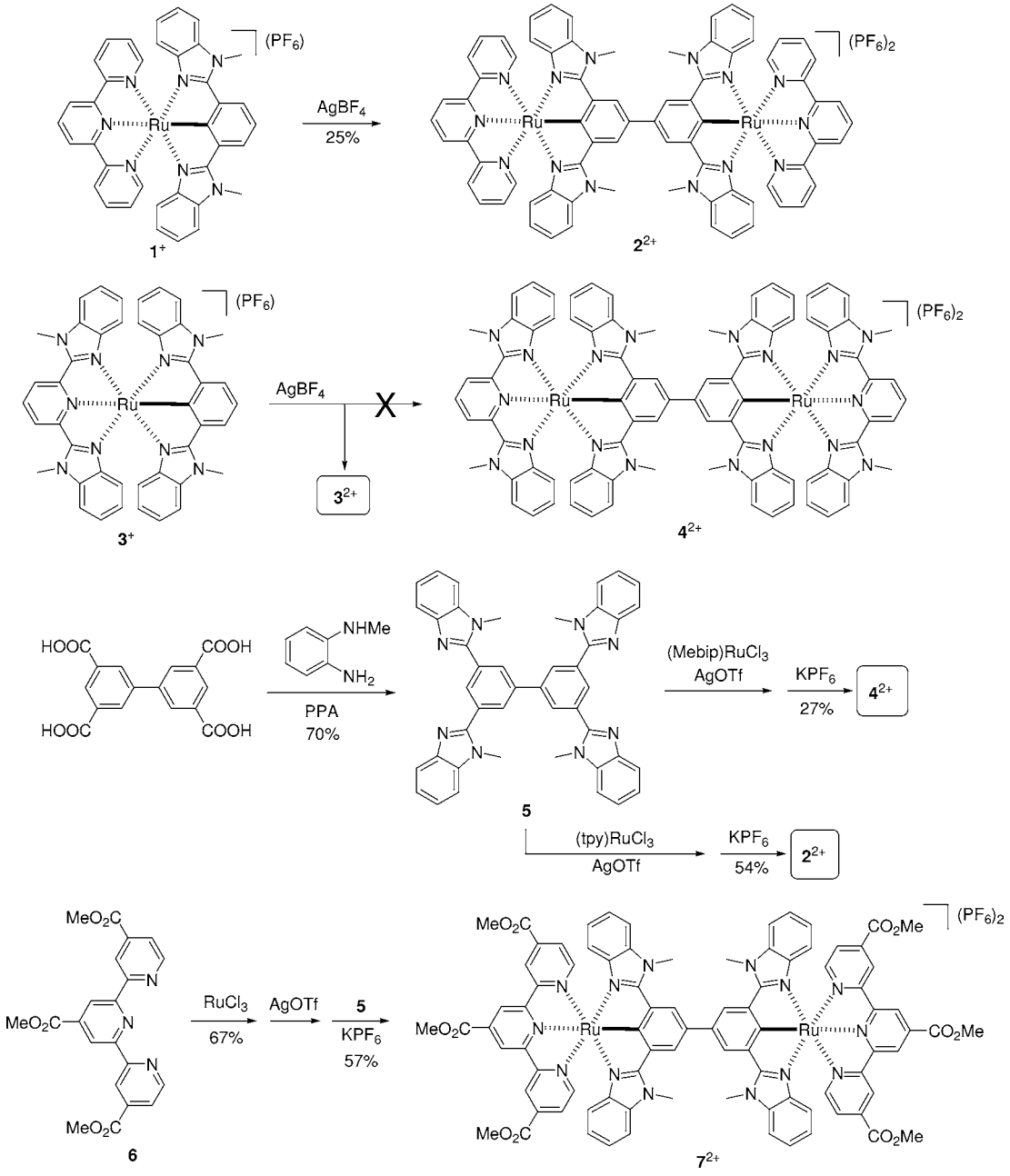

ligand **5**, which was obtained from the reaction of biphenyl-3,3′,5,5′-tetracarboxylic acid with *N*-methyl-1,2-phenylenediamine in good yield (70%). The reaction of 2 equiv of (Mebip)$RuCl_3$ with **5** in the presence of AgOTf, followed by a subsequent counteranion exchange, afforded the desired cyclometalated diruthenium complex $\mathbf{4}^{2+}$ in 27% yield. It should be noted that the diruthenium complex $\mathbf{2}^{2+}$ could also be prepared from the reaction of **5** with (tpy)$RuCl_3$ (tpy = 2,2′:6′,2″-terpyridine) in moderate yield, which actually is a better alternative to the synthesis of $\mathbf{2}^{2+}$ than the oxidative coupling method in our hand. Finally, a diruthenium complex $\mathbf{7}^{2+}$ capped with the electron-withdrawing ligands trimethyl-4,4′,4″-tricarboxylate-2,2′:6′,2″-terpyridine (Me_3tcbtpy) was prepared using the same method.

Electrochemical Studies. Electrochemical techniques, such as cyclic voltammetric (CV) and differential pulse voltammetric (DPV) analysis, are often used to qualitatively study the electronic coupling between metal centers of a series of structurally related dimetallic systems. A single metal-based two-electron redox wave suggests that the electronic coupling between two metals is weak. On the other hand, two separate sequential one-electron redox couples from the metals point to an efficient charge delocalization between them. However, electrochemical data are largely dependent on the measurement conditions, particularly the solvent and supporting electrolyte used.[18] This principle should be taken with great care.

The anodic CV and DPV profiles of $\mathbf{2}^{2+}$, $\mathbf{4}^{2+}$, and $\mathbf{7}^{2+}$ in *N*,*N*-dimethylformamide (DMF) are shown in Figure 1. Although these complexes have a common bridging ligand, their electrochemical properties are distinctly different. The capping ligands of different electronic properties make a big difference. Complex $\mathbf{2}^{2+}$ exhibits two sequential redox couples at +0.58 and +0.66 V vs Ag/AgCl with a potential difference (ΔE) of 76 mV between two half-wave

dx.doi.org/10.1021/ic300054j | *Inorg. Chem.* 2012, 51, 4343−4351

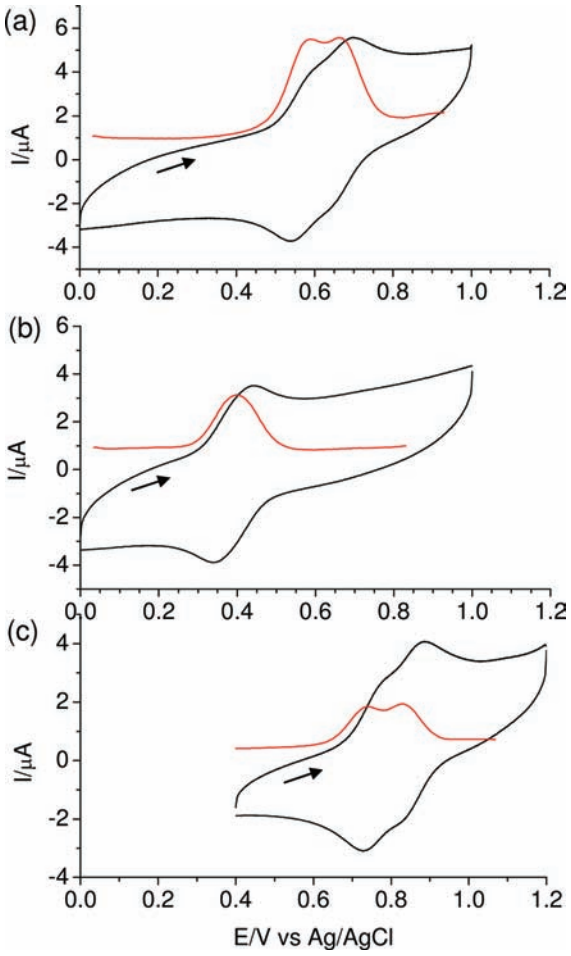

Figure 1. CV and DPV profiles of (a) $\mathbf{2}^{2+}$, (b) $\mathbf{4}^{2+}$, and (c) $\mathbf{7}^{2+}$ in DMF containing 0.1 M $^{n}Bu_4NClO_4$ at a scan rate of 100 mV/s. DPV was measured with a step potential of 5 mV and an amplitude of 50 mV. The working electrode was glassy carbon, the counter electrode was a platinum wire, and the reference electrode was Ag/AgCl in saturated aqueous NaCl. For CV profiles with wider potential windows, see Figures S1–S3 in the Supporting Information.

potentials. Complex $\mathbf{7}^{2+}$ capped with Me_3tctpy shows similar two waves at more positive potentials (+0.74 and +0.83 V) and with a slightly larger potential separation (ΔE = 88 mV). The comproportionation constants K_c for $\mathbf{2}^{2+}$ and $\mathbf{7}^{2+}$ were determined to be 20 and 31, respectively, according to the equation $K_c = 10^{\Delta E(\mathrm{mV})/59}$ for a room temperature case. However, complex $\mathbf{4}^{2+}$ with the electron-donating Mebip ligands only displays one reversible redox couple at +0.40 V, which should be associated with two inseparable one-electron waves. All of these peaks are attributed to the cyclometalated $Ru^{II/III}$ redox process mixing with some portion of ligand oxidation.[10−16] Complexes $\mathbf{2}^{2+}$ and $\mathbf{4}^{2+}$ exhibit a cathodic wave at −1.40 and −1.46 V vs Ag/AgCl, respectively (Figures S1 and S2 in the Supporting Information). They are ascribed to the reduction of corresponding capping ligands. However, reductions of the capping ligands of $\mathbf{7}^{2+}$ occur at much less negative potentials (−0.97 and −1.09 V vs Ag/AgCl; Figure S3 in the Supporting Information) because of their electron-withdrawing nature. The redox couples at the more negative potential in Figure S3 in the Supporting Information could be attributed to the reduction of the bridging ligand. These assignments are supported by theoretical calculations presented below.

Density Functional Theory (DFT) Calculations. DFT calculations were performed on the above complexes at the level of B3LYP/LANL2DZ/6-31G*/vacuum to study their electronic structures (see the Experimental Section for details). Selected frontier orbital structures with electron density distributions are shown in Figures S4–S7 in the Supporting Information and 2. The lowest unoccupied molecular orbitals

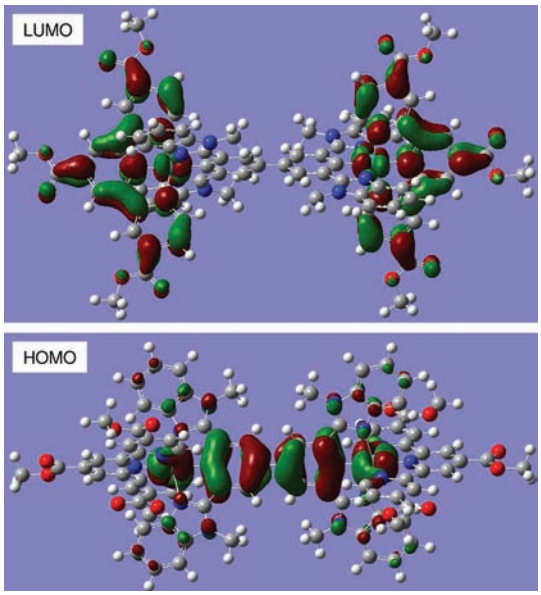

Figure 2. Isodensity plots of LUMO and HOMO for complex $\mathbf{7}^{2+}$. Calculation method: B3LYP/LANL2DZ/6-31G*/vacuum isovalue = 0.02.

(LUMOs) of all complexes are dominated by corresponding capping ligands. The highest occupied molecular orbitals (HOMOs) of all complexes have contributions from both the metal component and the center biphenyl backbone. A comparison of the Mulliken population of the HOMO compositions of three complexes is delineated in Table 1. For instance,

Table 1. Calculated Mulliken Population of HOMOs of the Complexes Studied

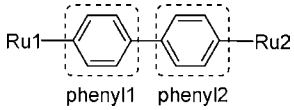

	Ru1	phenyl1	phenyl2	Ru2
$\mathbf{2}^{2+}$	0.22	0.19	0.19	0.22
$\mathbf{4}^{2+}$	0.22	0.19	0.17	0.22
$\mathbf{7}^{2+}$	0.21	0.19	0.19	0.21

complex $\mathbf{2}^{2+}$ has populations of 0.22 and 0.19 for each Ru atom and bridging phenyl ring, respectively. Complexes $\mathbf{4}^{2+}$ and $\mathbf{7}^{2+}$ have similar HOMO compositions. This suggests that the bridging biphenyl unit accounts for a considerable HOMO composition for these complexes, and the electrochemical waves shown in Figure 1 are a result of oxidation of both ruthenium and the biphenyl backbone. This feature has been previously found for many biscyclometalated ruthenium complexes.[5,12,13]

The calculated energy-level alignment of the above complexes is shown in Figure 3. Compared to that of $\mathbf{2}^{2+}$, the HOMO of $\mathbf{4}^{2+}$ is destabilized and the HOMO of $\mathbf{7}^{2+}$ is stabilized. This correlates well with the electrochemical behavior of these complexes (Figure 1). In comparison, complex $\mathbf{7}^{2+}$ has the smallest energy gap (2.50 eV).

dx.doi.org/10.1021/ic300054j | Inorg. Chem. 2012, 51, 4343−4351

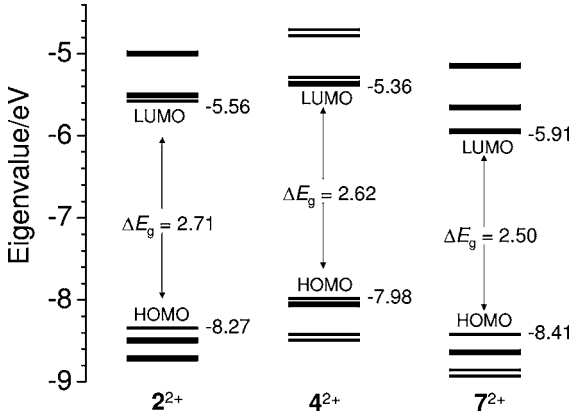

Figure 3. Energy-level alignment diagram of the complexes calculated.

Because of the electron-withdrawing nature of the capping ligand of 7^{2+}, the degree of LUMO stabilization is larger than that of the HOMO, which results in a decrease of the energy gap of 7^{2+} compared to that of 2^{2+} or 4^{2+}. This is also reflected in their absorption spectra presented below.

Electronic Absorption Spectra and Time-Dependent DFT (TDDFT) Calculations. The electronic absorption spectra of the dimetallic complexes 2^{2+}, 4^{2+}, and 7^{2+} are shown in Figure 4, together with those of the monometallic complexes 1^{+} and 3^{+} for comparison. Absorptions in the UV and visible regions are ascribed to the intraligand (IL) $\pi-\pi^*$ transition of both cyclometalating and auxiliary ligands and metal-to-ligand charge-transfer (MLCT) transitions, respectively. The shapes and energies of the absorptions of 2^{2+} and 4^{2+} resemble those of 1^{+} and 3^{+}, respectively, albeit with an increase in the molar absorptivities and a slight red shift of the MLCT transitions. For instance, the main MLCT peaks of 2^{2+} and 4^{2+} center at 520 and 528 nm, respectively, which are slightly bathochromically shifted compared to those of 1^{+} and 3^{+} (500 and 512 nm, respectively). The MLCT transitions of 1^{+} and 3^{+} have been previously analyzed in great detail with the aide of TDDFT calculations.[11] We believe that the same assignments should also be applicable to 2^{2+} and 4^{2+}. For complex 2^{2+}, the band at 520 nm is attributed to both the bridging-ligand- and tpy-targeted MLCT transitions, and the former plays a more important role. The peak at 395 nm is mainly associated with the tpy-targeted MLCT transitions. For complex 4^{2+}, the visible band between 400 and 600 nm is associated with both the bridging-ligand- and Mebip-targeted MLCT transitions. The absorption features of 7^{2+} are somewhat different from others. We performed TDDFT calculations on the DFT-optimized structure of 7^{2+} at the level of B3LYP/LANL2DZ/6-31G*/CPCM/CH_3CN theory (see the Experimental Section) to help assign its absorption (Table S1 in the Supporting Information). The involved molecular orbital diagrams are given in Figures S6 and S7 in the Supporting Information. As can be found from Figure 4b, the strengths of the predicted excitations agree well with the observed absorption spectrum of 7^{2+}. However, the energies of the predicted excitations are blue-shifted by about 30–40 nm. The broad and shallow absorption at 720 nm is mainly associated with the HOMO−2 → LUMO and HOMO−1 → LUMO+1 excitations (S2 in Table S1, Supporting Information). They can be interpreted as the capping-ligand-targeted MLCT transitions. Absorption bands between 510 and 660 nm have similar MLCT character from HOMO−5 → LUMO+2, HOMO−4 → LUMO+3, HOMO−1 → LUMO+3, and HOMO−2 → LUMO+2 excitations (S12 and S15 in Table S1, Supporting Information). As far as the intense absorption band between 380 and 510 nm is concerned, in addition

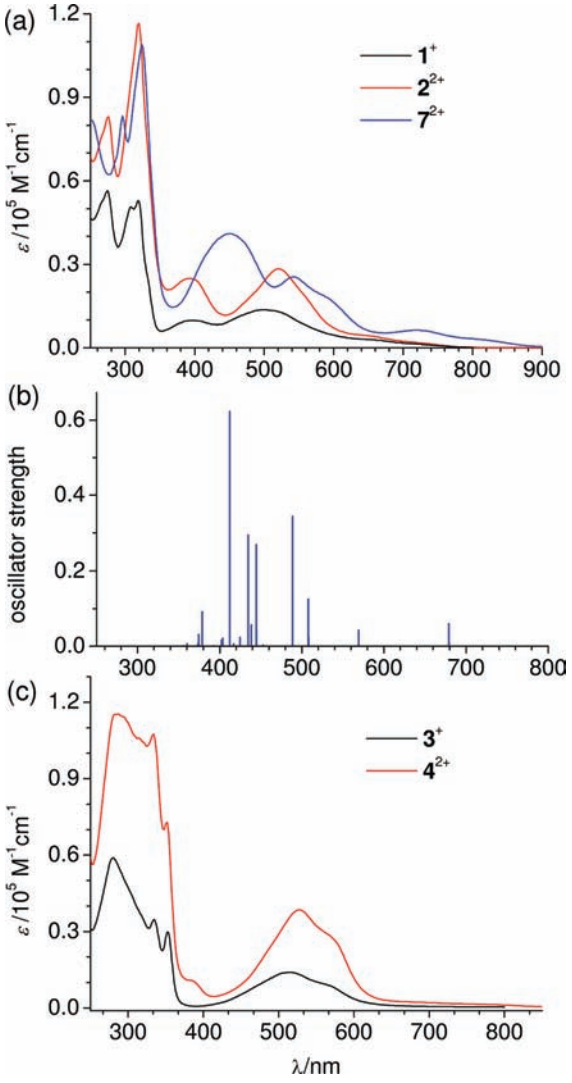

Figure 4. (a) Electronic absorption spectra of 1^{+} (black line), 2^{2+} (red line), and 7^{2+} (blue line) in acetonitrile. (b) TDDFT-predicted vertical excitations of 7^{2+}. (c) Electronic absorption spectra of 3^{+} (black line) and 4^{2+} (red line) in acetonitrile.

to the capping ligand, the bridging-ligand-targeted MLCT transitions make a big contribution as well (LUMO+8 and LUMO+9). The red shift of the observed MLCT transitions of 7^{2+} vs 2^{2+} or 4^{2+} is consistent with its reduced energy gap, as inferred from the above DFT calculations.

Near-Infrared (NIR) Transition Analysis of MV Species. MV systems often display a characteristic intervalence charge-transfer (IVCT) band in the NIR region, which is not observable in corresponding homovalent complexes. The degree of electronic coupling of MV systems can be estimated on the basis of the IVCT band analysis. The visible (vis)/NIR absorption spectral changes of complexes 2^{2+}, 4^{2+}, and 7^{2+} upon oxidative titration with cerium ammonium nitrate (CAN) are shown in Figure 5. Table 2 summarizes the parameters obtained upon IVCT analysis. When a solution of 2^{2+} in acetonitrile was gradually treated with up to 1 equiv of CAN, MLCT transitions in the visible decreased a little. At the same time, the emergence of a broad absorption band in the NIR region was evident (Figure 5a). When the amount of CAN was gradually increased to 2 equiv, MLCT transitions continued to decrease and the new NIR band decreased gradually as well until it disappeared completely (Figure 5b). Thus, this new NIR band specifically

dx.doi.org/10.1021/ic300054j | Inorg. Chem. 2012, 51, 4343–4351

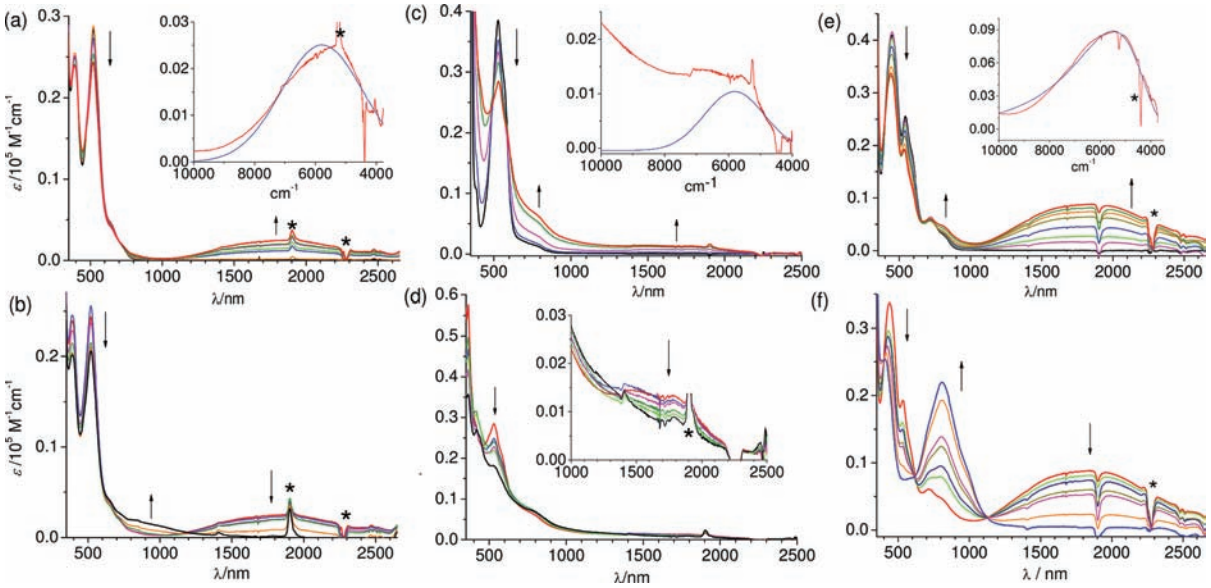

Figure 5. Absorption spectral changes of (a and b) ruthenium complexes $\mathbf{2}^{2+}$, (c and d) $\mathbf{4}^{2+}$, and (e and f) $\mathbf{7}^{2+}$ in acetonitrile upon first-electron (a, c, and e) and second-electron (b, d, and f) oxidation by adding different equivalents of CAN while keeping the concentrations of $\mathbf{2}^{2+}$, $\mathbf{4}^{2+}$, or $\mathbf{7}^{2+}$ constant. Shown in insets of a, c, and e are NIR bands of $\mathbf{2}^{3+}$, $\mathbf{4}^{3+}$, or $\mathbf{7}^{3+}$ with Gaussian-fitted lines (blue lines) as a function of the wavenumbers, respectively. Asterisks denote artifacts due to nonperfect background compensation.

Table 2. Parameters for the IVCT Transitions of the Complexes Studied

	λ_{max}/nm	ν_{max}/cm^{-1}	ε_{max} (M^{-1} cm^{-1})	$\Delta\nu_{1/2}$(exp) (cm^{-1})	$\Delta\nu_{1/2}$(theo) (cm^{-1})[a]	Γ[b]	r_{ab} (Å)	H_{ab} (cm^{-1})[c]
$\mathbf{2}^{3+}$	1730	5780	2500	3170	3654	0.13	11.16	395
$\mathbf{4}^{3+}$	1715	5830	1040	2140	3670	0.72	11.15	210
$\mathbf{7}^{3+}$	1828	5470	8875	3330	3555	0.063	11.17	740

[a]The theoretical $\Delta\nu_{1/2}$ value equals $(2310\nu_{max})^{1/2}$. [b]$\Gamma = 1 - \Delta\nu_{1/2exp}/\Delta\nu_{1/2theo}$. [c]$H_{ab} = 0.0206(\varepsilon_{max}\nu_{max}\Delta\nu_{1/2})^{1/2}/r_{ab}$ for a Robin and Day class II system.

associated with the one-electron-oxidized species $\mathbf{2}^{3+}$ is attributed to the IVCT transition. It should also be mentioned that a new shoulder band around 900 nm is observable in Figure 5b, which is ascribed to the ligand-to-metal charge-transfer transition. A Gaussian-fitted line of the IVCT band is shown in the inset of Figure 5a. The observed full width at half-height ($\Delta\nu_{1/2}$) is 3170 cm^{-1}. The theoretical $\Delta\nu_{1/2}$ value of this band is determined to be 3654 cm^{-1}, according to Hush's expression [$\Delta\nu_{1/2theo} = (2310\nu_{max})^{1/2}$],[19] which is slightly wider than the experimental $\Delta\nu_{1/2}$ value. The Γ parameter, introduced by Sutin and co-workers,[20] of this band is 0.13, as determined by $\Gamma = 1 - \Delta\nu_{1/2exp}/\Delta\nu_{1/2theo}$.

The vis/NIR absorption spectral changes of $\mathbf{4}^{2+}$ and $\mathbf{7}^{2+}$ upon oxidative titration with CAN are shown in Figure 5c–f, which evidence the appearance and disappearance of the IVCT band in a similar region. However, it is clear that MV complex $\mathbf{4}^{3+}$ displays a much weaker IVCT band, while $\mathbf{7}^{3+}$ exhibits a much more intense one (ε_{max} = 8875 M^{-1} cm^{-1}) than that of $\mathbf{2}^{3+}$. The stepwise oxidation process of 7 ($\mathbf{7}^{2+} \rightarrow \mathbf{7}^{3+} \rightarrow \mathbf{7}^{4+}$) could also be realized by the electrochemical method in different solvents (Figures S8–S10 in the Supporting Information). For instance, when a solution of $\mathbf{7}^{2+}$ in acetonitrile containing 0.1 M $^{n}Bu_4ClO_4$ was stepwise applied, with a potential from +0.4 to +0.75 V vs Ag/AgCl with an indium–tin oxide glass electrode, the first-electron-oxidation process took place smoothly, as evidenced by the appearance of the IVCT band in the NIR region (Figure S8a in the Supporting Information). When the potential was further increased to induce the second-electron oxidation, the disappearance of the IVCT band was observed (Figure S8b in the Supporting Information). Figure 6 shows a comparison of the IVCT bands of $\mathbf{7}^{3+}$ in different solvents

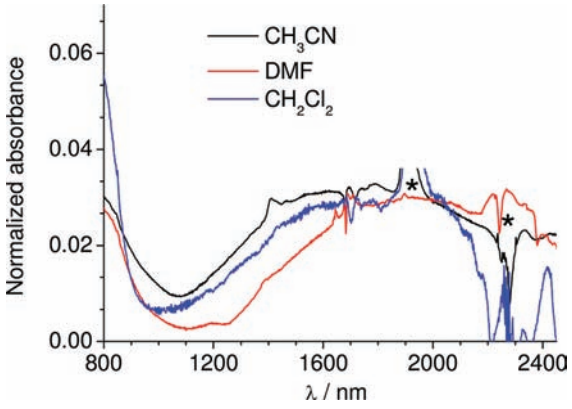

Figure 6. NIR electronic absorption spectra of $\mathbf{7}^{3+}$ in different solvents obtained in spectroelectrochemical measurements. *: Artifacts caused by a nonperfect background compensation.

studied (CH_3CN, DMF, and CH_2Cl_2), which proved that the IVCT bands in CH_3CN and CH_2Cl_2 had similar energies and shapes. However, the energy of the IVCT band in DMF is distinctly red-shifted. The spectroelectrochemical measurements of $\mathbf{2}^{2+}$ and $\mathbf{4}^{2+}$ did not proceed well because of their limited solubility in the presence of the electrolyte. On the basis of these analyses, we conclude that $\mathbf{2}^{3+}$ and $\mathbf{4}^{3+}$ are Robin and Day class II systems, while $\mathbf{7}^{3+}$ is either a class II system or on the II/III borderline. The electronic coupling parameters (H_{ab}) of $\mathbf{2}^{3+}$, $\mathbf{4}^{3+}$, and $\mathbf{7}^{3+}$ were thus calculated to be 395, 210, and 740 cm^{-1}, respectively, according to

dx.doi.org/10.1021/ic300054j | Inorg. Chem. 2012, 51, 4343–4351

the Hush formula[21] $H_{ab} = 0.0206(\varepsilon_{max}\nu_{max}\Delta\nu_{1/2})^{1/2}/r_{ab}$, where r_{ab} was taken to be the DFT-calculated Ru−Ru distance.

As can be seen from the above analysis, the intermetallic electronic coupling of the complexes studied is in the order of 7^{3+} > 2^{3+} > 4^{3+}. The effect of the terminal ligands on the electronic coupling process at the MV state has been previously demonstrated.[22] In a similar MV system with cyclometalated rutheniums as the charge-bearing sites, Launay and co-workers found that the presence of electron-rich *tert*-butyl groups on the terminal ligands reduced the intermetallic coupling,[13a] which coincides with our results. To further aid in the understanding of the electron-transfer processes in these systems, DFT calculations on the open-shell complexes 2^{3+}, 4^{3+}, and 7^{3+} were preformed on the level of UB3LYP/LanL2DZ/6-31G*/vacuum theory with the input files generated from the previously DFT-optimized structures of 2^{2+}, 4^{2+}, and 7^{2+}. The dihedral angles between two central phenyl rings of 2^{2+}, 4^{2+}, and 7^{2+} are 43.48°, 45.93°, and 43.92°, respectively. In the open-shell complexes 2^{3+} and 4^{3+}, these angles decrease to 34.53° and 34.57°, respectively. However, this angle increases to 47.53° in the case of 7^{3+}, which is appreciably larger than those of 2^{3+} and 4^{3+}. These results contradict a common sense that a more planar bridge enhances an electron-transfer process because complex 7^{3+} with the biggest dihedral angle exhibits the strongest electron coupling among the three complexes studied.

The spin-density plots of 2^{3+}, 4^{3+}, and 7^{3+} are shown in Figure 7. Table 3 summarizes the Mulliken spin-density populations of three

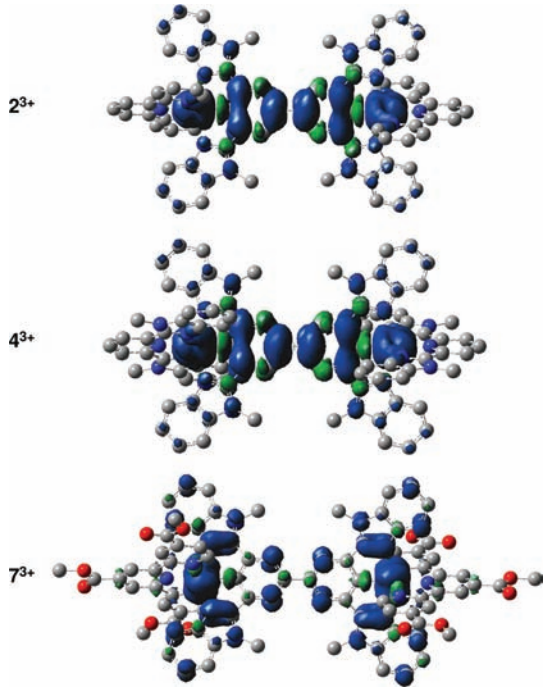

Figure 7. Spin-density plots of 2^{3+}, 4^{3+}, and 7^{3+}. H atoms are omitted for clarity.

complexes. The free spins in 2^{3+} and 4^{3+} are delocalized across the Ru−biphenyl−Ru array. Each Ru atom and phenyl ring in 2^{3+} has spin populations of 0.338 and 0.126, respectively. In the complex 4^{3+} with electron-rich Mebip terminal ligands, the phenyl rings have even larger contributions (0.145 each). Although DFT methods have an artificial preference for delocalization,[23] it does suggest that appreciable amounts of spin in 2^{3+} and 4^{3+} are associated with the biphenyl backbone. This phenomenon has been previously

Table 3. Calculated Spin-Density Distributions of 2^{3+}, 4^{3+}, and 7^{3+} on the Level of UB3LYP/LanL2DZ/6-31G*/Vacuum[a]

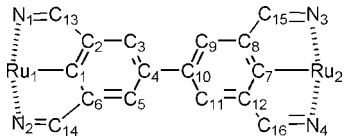

atom	spin density		
	2^{3+}	4^{3+}	7^{3+}
Ru_1	0.338	0.319	0.406
Ru_2	0.338	0.320	0.406
C_1	−0.020	−0.024	−0.011
C_2	0.054	0.061	−0.006
C_3	−0.014	−0.013	0.019
C_4	0.066	0.073	−0.009
C_5	−0.014	−0.013	0.019
C_6	0.054	0.061	−0.006
$C_{1+2+3+4+5+6}$	0.126	0.145	0.006
C_7	−0.020	−0.024	−0.011
C_8	0.054	0.061	−0.006
C_9	−0.014	−0.013	0.019
C_{10}	0.066	0.073	−0.009
C_{11}	−0.014	−0.013	0.019
C_{12}	0.054	0.061	−0.006
$C_{7+8+9+10+11+12}$	0.126	0.145	0.006
N_1, N_2, N_3, or N_4	0.004	0.006	0.016
C_{13}, C_{14}, C_{15}, or C_{16}	−0.015	−0.016	0.011

[a]The spin density is determined by the difference of the Mulliken charges of α and β electrons ($\alpha - \beta$).

observed in many biscyclometalated complexes.[5,13−16] In stark contrast, complex 7^{3+} has dominant spin contributions from two metal centers (0.406 each). The spin distribution on the biphenyl fragment is negligible. The smaller dihedral angles between two central phenyl rings of 2^{3+} and 4^{3+} than that of 7^{3+} is caused by the spin delocalization in 2^{3+} and 4^{3+}. Electron paramagnetic resonance (EPR) analysis can provide useful information on the spin distributions of metal complexes. However, to our disappointment, we failed to obtain distinct EPR signals for complexes 2^{3+}, 4^{3+}, and 7^{3+} even at 77 K. The calculated spin distributions of 2^{3+}, 4^{3+}, and 7^{3+} shown in Figure 7 seem in contradiction with the experimental findings at the first sight. Complexes 2^{3+} and 4^{3+} exhibit a large degree of spin delocalization, but their electronic couplings are much weaker than 7^{3+} according to the above IVCT band analysis. However, we should keep in mind that the spin delocalization across the bridge does not necessarily stand for a strong electronic coupling between two termini, but it does mean that some amount of the bridge participates in the involved oxidation process. For delocalized systems with conventional noncyclometalated rutheniums as the redox centers, the bridge does not contribute to the spin distribution.

The electron-transfer processes in these complexes could be rationalized by a hole-transfer-tunneling mechanism. In the electron-tunneling regime, two transfer processes could be envisaged: electron-transfer or hole-transfer superexchange[24] (Figure S11 in the Supporting Information). In the electron-transfer mechanism, the electron moves from the donor state to the LUMO of the bridge, followed by subsequent transfer to the acceptor state. On the other hand, if the process is initiated from the electron transfer from the bridge's HOMO to the acceptor state, it is termed the hole-transfer superexchange

dx.doi.org/10.1021/ic300054j | Inorg. Chem. 2012, 51, 4343−4351

mechanism. Qualitatively speaking, the smaller the energy gap between the donor state and LUMO of the bridge (ΔE_{ET}), the more important role the electron-transfer superexchange will play. On the other hand, the smaller the energy difference between the acceptor state and HOMO of the bridge (ΔE_{HT}), the bigger contribution the hole-transfer superexchange will make. In the biphenyl-bridged biscyclometalated ruthenium series, there is a strong orbital overlap between metals and bridging ligands and the energy gap between them is small because of the anionic nature of the bridging ligand.[5,10−16] Thus, a hole-transfer superexchange is believed to play a more important role in the series $\mathbf{2}^{3+}$, $\mathbf{4}^{3+}$, and $\mathbf{7}^{3+}$ with a similar bridging state. Figure S12 in the Supporting Information shows the highest single occupied molecular orbital isodensity plots of $\mathbf{2}^{3+}$, $\mathbf{4}^{3+}$, and $\mathbf{7}^{3+}$, which are very similar to the HOMOs of $\mathbf{2}^{2+}$, $\mathbf{4}^{2+}$, and $\mathbf{7}^{2+}$. In the case of the complex $\mathbf{4}^{3+}$ with electron-donating benzimidazole capping ligands, the donor or acceptor state is destabilized more than that of $\mathbf{2}^{3+}$ (as has been discussed in the electrochemical analysis and DFT results). As a result, the ΔE_{HT} value increases and the intermetallic coupling becomes weaker. For the same reason, complex $\mathbf{7}^{3+}$ with electron-withdrawing capping ligands leads to the decrease of the ΔE_{HT} value and the increase of the electronic coupling. We know from these results that the ΔE_{HT} value plays a more important role than the planarity of the bridge on the degree of the electronic coupling in these complexes.

CONCLUSION

To summarize, we present in this contribution the studies of a series of biscyclometalated ruthenium complexes bridged by the title ligand. A combination of electrochemical, spectroscopic, DFT, and IVCT transition analysis proved that the electronic nature of capping ligands plays a very important role in determining the electronic coupling degree of these MV complexes. Complex $\mathbf{4}^{3+}$ with electron-rich benzimidazole capping ligands exhibits a weaker coupling, while complex $\mathbf{7}^{3+}$ with electron-deficient capping ligands shows an enhanced electronic coupling. This trend can be rationalized on the basis of a hole-transfer-tunneling mechanism. Although biscyclometalated ruthenium systems bridged with various conjugated ligands have been reported in many publications,[5,12−16] the effect of the capping ligand on the degree of intermetallic electronic coupling has not been examined in depth. Our results presented in this paper are believed to greatly stimulate such studies. In addition, cyclometalated ruthenium complexes have recently been investigated as promising NIR electrochromic materials[25] and efficient sensitizers for solar cell applications.[26] Compounds described in this paper, especially complex 7 with the capping ligands Me_3tcbtpy that can be converted into carboxylic acid anchor groups after a simple transformation,[26c] exhibited interesting vis/NIR absorption features under different oxidation states and will be useful for such purposes.

EXPERIMENTAL SECTION

Spectroscopic Measurements. All optical ultraviolet/visible (UV/vis) absorption spectra were obtained using a TU-1810DSPC spectrometer of Beijing Purkinje General Instrument Co. Ltd. at room temperature in denoted solvents, with a conventional 1.0 cm quartz cell. UV/vis/NIR spectra were recorded using a PE Lambda 750 UV/vis/NIR spectrophotometer.

Electrochemical Measurements. All cyclic voltammograms were taken using a CHI620D potentiostat. All measurements were carried out in 0.1 M of Bu_4NClO_4/DMF at a scan rate of 100 mV/s with a Ag/AgCl reference electrode. The working electrode was glassy carbon, and a platinum coil was used as the counter electrode.

Computational Methods. DFT calculations were carried out using the B3LYP exchange correlation functional[27] and implemented in the *Gaussian 03* program package.[28] The electronic structures of the complexes were determined using a general basis set with the Los Alamos effective core potential LanL2DZ basis set for ruthenium[29] and 6-31G* for other atoms in vacuum.[30] In the case where the solvation effects are included, the conductor-like polarizable continuum model (CPCM) with acetonitrile as the solvent and united-atom Kohn−Sham radii were employed.[31]

Synthesis. NMR spectra were recorded in the designated solvent on a Bruker Avance 400 MHz spectrometer. Spectra are reported in ppm values from residual protons of the deuterated solvent for ^{1}H NMR (7.26 ppm for $CDCl_3$ and 1.92 ppm for CD_3CN). Mass spectrometry (MS) data were obtained with a Bruker Daltonics Inc. Apex II FT-ICR or Autoflex III MALDI-TOF mass spectrometer. The matrix for matrix-assisted laser desorption ionization time-of-flight (MALDI-TOF) measurement is α-cyano-4-hydroxycinnamic acid. Microanalysis was carried out using a Flash EA 1112 or Carlo Erba 1106 analyzer at the Institute of Chemistry, Chinese Academy of Sciences.

Synthesis of [2](PF$_6$)$_2$. To 15 mL dry of ^{n}BuOH were added [Ru(tpy)(Mebib)](PF$_6$)[11a] ($\mathbf{1}^+$; 62.5 mg, 0. 77 mmol) and $AgBF_4$ (151.3 mg, 0.77 mmol). The mixture was refluxed for 5 h. After cooling to room temperature, the solvent was removed under reduced pressure, and the residue was dissolved in a proper amount of methanol. After the addition of an excess of KPF_6, the resulting precipitate was collected by filtration and washing with water and Et_2O successively. The obtained solid was subjected to flash column chromatography on silica gel (eluent: CH_3CN/H_2O/aqueous KNO_3, 100/10/0.2) followed by anion exchange with KPF_6 to give 15.6 mg of $[\mathbf{2}](\mathbf{PF_6})_2$ in a yield of 25%. ^{1}H NMR (400 MHz, CD_3CN): δ 4.55 (s, 12H), 5.83 (d, J = 8.4 Hz, 4H), 6.83 (t, J = 7.7 Hz, 4H), 7.00 (t, J = 6.5 Hz, 4H), 7.14 (t, J = 7.6 Hz, 4H), 7.35 (d, J = 5.5 Hz, 4H), 7.48 (d, J = 7.9 Hz, 4H), 7.62 (t, J = 7.6 Hz, 4H), 8.38 (d, J = 8.0 Hz, 4H), 8.43 (d, J = 7.8 Hz, 2H), 8.84 (d, J = 8.3 Hz, 4H), 8.98 (s, 4H). MALDI-TOF for $[M - PF_6 - H]^+$: m/z 1485.0 (calcd m/z 1485.23). Anal. Calcd for $C_{74}H_{54}F_{12}N_{14}P_2Ru_2{\cdot}2H_2O$: C, 53.30; H, 3.51; N, 11.76. Found: C, 53.20; H, 3.42; N, 11.62. Complex $[\mathbf{2}](\mathbf{PF_6})_2$ was also prepared in a yield of 54% starting from Ru(tpy)Cl_3 and **5** in a procedure similar to that for the synthesis of $[\mathbf{4}](\mathbf{PF_6})_2$ as shown below.

Synthesis of 5. A mixture of biphenyl-3,3′,5,5′-tetracarboxylic acid (100 mg, 0.3 mmol) and *N*-methyl-1,2-phenylenediamine (250 mg, 1.28 mmol) in 10 mL of polyphosphoric acid was stirred at ca. 210 °C for 8 h. After cooling to room temperature, the reaction mixture was poured into 30 mL of water and neutralized by a 5 M aqueous NaOH solution. The resulting precipitate was collected by filtration and washing with water. The obtained crude product was subjected to flash column chromatography on silica gel (eluent: CH_2Cl_2/acetone, 1/1) to give 142 mg of compound **5** as a slightly yellow solid in a yield of 70%. ^{1}H NMR (400 MHz, $CDCl_3$): δ 3.97 (s, 12H), 7.36 (m, J = 6.6 Hz, 8H), 7.44 (d, J = 7.4 Hz, 4H), 7.85 (d, J = 7.4 Hz, 4H), 8.17 (s, 2H), 8.29 (s, 4H). EI-MS: m/z 673 for $[M - H]^+$. EI-HRMS. Calcd for $C_{44}H_{33}N_8$: m/z 673.2828. Found: m/z 673.2838.

Synthesis of [4](PF$_6$)$_2$. To 10 mL of dry acetone were added Ru(Mebip)Cl_3[11b] (55 mg, 0.1 mmol) and AgOTf (80 mg, 0.31 mmol). The mixture was refluxed for 2 h before cooling to room temperature. The precipitate was removed by filtration, and the filtrate was concentrated to dryness. To the residue were added 3,3′,5,5′-tetrakis (1-methylbenzimidazol-2-yl)biphenyl (33 mg, 0.05 mmol), DMF (10 mL), and ^{t}BuOH (10 mL). The mixture was then refluxed for another 24 h. After cooling to room temperature, the solvent was removed under reduced pressure. The residue was dissolved in a proper amount of methanol. After the addition of an excess of KPF_6, the resulting precipitate was collected by filtration and washing with water and Et_2O. The obtained solid was subjected to flash column chromatography on silica gel (eluent: CH_3CN/H_2O/aqueous KNO_3, 100/10/0.1) followed by anion exchange with KPF_6 to give 25 mg of $[\mathbf{4}](\mathbf{PF_6})_2$ in a yield of 27%. MALDI-TOF for $[M - 2PF_6 - CH_3 - H]^{2+}$: m/z 1537.9 (calcd m/z 1538.35). Anal. Calcd for $C_{86}H_{66}F_{12}N_{18}P_2Ru_2{\cdot}2H_2O{\cdot}Et_2O$: C, 55.33; H, 4.13; N, 12.90. Found: C, 55.33; H, 4.18; N, 12.59.

dx.doi.org/10.1021/ic300054j | Inorg. Chem. 2012, 51, 4343−4351

Synthesis of [7](PF$_6$)$_2$. To 40 mL of ethanol were added 405 mg of $RuCl_3 \cdot 3H_2O$ and 265 mg of Me_3tctpy. The mixture was refluxed for 8 h before cooling to room temperature. The resulting precipitate was collected by filtration and washing with water to give 412.2 mg of Ru(Me_3tctpy)Cl_3 (67%), which was used for the next transformation without further purification. To 10 mL of dry acetone were added Ru(Me_3tctpy)Cl_3 (64.6 mg, 0.105 mmol) and AgOTf (100 mg, 0.38 mmol). The mixture was refluxed for 2 h before cooling to room temperature. The AgCl precipitate was removed by filtration, and the filtrate was concentrated to dryness. To the residue were added **5** (35 mg, 0.052 mmol), DMF (10 mL), and ^{t}BuOH (10 mL). The mixture was then refluxed for 24 h under a nitrogen atmosphere. After cooling to room temperature, the solvent was removed under reduced pressure. The residue was dissolved in a proper amount of methanol, followed by the addition of an excess of KPF_6. The resulting precipitate was collected by filtration and washing with water and Et_2O. The obtained solid was subjected to flash column chromatography on silica gel (eluent: CH_3CN/H_2O/aqueous KNO_3, 100/10/0.2) to give 59 mg of [7](**PF$_6$**)$_2$ (57%). MALDI-TOF for $[M - PF_6 - 2H]^+$: *m*/*z* 1834.8 (calcd *m*/*z* 1835.26). Anal. Calcd for $C_{86}H_{66}F_{12}N_{14}O_{12}P_2Ru_2 \cdot 4H_2O$: C, 50.35; H, 3.64; N, 9.56. Found: C, 50.07; H, 3.70; N, 9.67.

■ ASSOCIATED CONTENT

Supporting Information

CV profiles of 2^{2+}, 4^{2+}, and 7^{2+} with a wider potential window, DFT/TDDFT calculation results, oxidative spectroelectrochemistry of 7^{2+}, an electron-transfer versus hole-transfer superexchange mechanism, and SOMO surfaces. This material is available free of charge via the Internet at http://pubs.acs.org.

■ AUTHOR INFORMATION

Corresponding Author

*E-mail: zhongyuwu@iccas.ac.cn.

Notes

The authors declare no competing financial interest.

■ ACKNOWLEDGMENTS

We thank the National Natural Science Foundation of China (Grant 21002104), the National Basic Research 973 program of China (Grant 2011CB932301), the Scientific Research Foundation for the Returned Overseas Chinese Scholars, State Education Ministry of China, and the Institute of Chemistry, Chinese Academy of Sciences ("100 Talent" Program), for financial support.

■ REFERENCES

(1) (a) Creutz, C.; Taube, H. *J. Am. Chem. Soc.* **1969**, *91*, 3988. (b) Creutz, C.; Taube, H. *J. Am. Chem. Soc.* **1973**, *95*, 1086.

(2) (a) D'Alessandro, D. M.; Keene, F. R. *Chem. Rev.* **2006**, *106*, 2270. (b) Kaim, W.; Lahiri, G. K. *Angew. Chem., Int. Ed.* **2007**, *46*, 1778. (c) D'Alessandro, D. M.; Keene, F. R. *Chem. Soc. Rev.* **2006**, *35*, 424. (d) Aguirre-Etcheverry, P.; O'Hare, D. *Chem. Rev.* **2010**, *110*, 4839. (e) Demadis, K. D.; Hartshorn, C. M.; Meyer, T. J. *Chem. Rev.* **2001**, *101*, 2655. (f) Kaim, W.; Klein, A.; Glöckle, M. *Acc. Chem. Res.* **2000**, *33*, 755.

(3) (a) Semenov, S. N.; Blacque, O.; Fox, T.; Venkatesan, K.; Berke, H. *J. Am. Chem. Soc.* **2010**, *132*, 3115. (b) Li, Y.; Joscowicz, M.; Tolbert, L. M. *J. Am. Chem. Soc.* **2010**, *132*, 10374. (c) Kundu, T.; Sarkar, B.; Mondal, T. K.; Fiedler, J.; Mobin, S. M.; Kaim, W.; Lahiri, G. K. *Inorg. Chem.* **2010**, *49*, 6565. (d) Hildebrandt, A.; Schaarschmidt, D.; Lang, H. *Organometallics* **2011**, *30*, 556. (e) Bunting, P.; Chisholm, M. H.; Gallucci, J. C.; Lear, B. J. *J. Am. Chem. Soc.* **2011**, *133*, 5873. (f) Yao, C.-J.; Yao, J.; Zhong, Y.-W. *Inorg. Chem.* **2011**, *50*, 6847. (g) Nie, H.-J.; Yao, C.-J.; Yao, J.; Zhong, Y.-W. *Chem. Asian J.* **2011**, *6*, 3322.

(4) Robin, M. B.; Day, P. *Adv. Inorg. Chem. Radiochem.* **1967**, *8*, 357.

(5) (a) Wadman, S. H.; Lutz, M.; Tooke, D. M.; Spek, A. L.; Hartl, F.; Havenith, R. W. A.; van Klink, G. P. M.; van Koten, G. *Inorg. Chem.* **2009**, *48*, 1887. (b) Fox, M. A.; Robert, R. L.; Baines, T. E.; Guennic, B. L.; Halet, J.-F.; Hartl, F.; Yufit, D. S.; Albesa-Jové, D.; Howard, J. A. K.; Low, P. J. *J. Am. Chem. Soc.* **2008**, *130*, 3566. (c) Jäger, M.; Smeigh, A.; Lombeck, F.; Görls, H.; Collin, J.-P.; Sauvage, J.-P.; Hammarström, L.; Johannsson, O. *Inorg. Chem.* **2010**, *49*, 374. (d) Wu, S.-H.; Burkhardt, S. E.; Yao, J.; Zhong, Y.-W.; Abruña, H. D. *Inorg. Chem.* **2011**, *50*, 3959. (e) Zhong, Y.-W.; Wu, S.-H.; Burkhardt, S. E.; Yao, C.-J.; Abruña, H. D. *Inorg. Chem.* **2011**, *50*, 517. (f) Fox, M. A.; Le Guennic, B.; Roberts, R. L.; Brue, D. A.; Yufit, D. S.; Howard, J. A. K.; Manca, G.; Halet, J.-F.; Hartl, F.; Low, P. J. *J. Am. Chem. Soc.* **2011**, *133*, 18433. (g) Xi, B.; Liu, I. P.-C.; Xu, G.-L.; Choudhuri, M. M. R.; DeRosa, M. C.; Crutchley, R. J.; Ren, T. *J. Am. Chem. Soc.* **2011**, *133*, 15094. (h) Malvolti, F.; Rouxel, C.; Mongin, O.; Hapiot, P.; Toupet, L.; Blanchard-Desce, M.; Paul, F. *Dalton Trans.* **2011**, *40*, 6616.

(6) (a) Aquino, M. A. S.; Lee, F. L.; Gabe, E. J.; Bensimon, C.; Greedan, J. E.; Crutchley, R. J. *J. Am. Chem. Soc.* **1992**, *114*, 5130. (b) Mosher, P. J.; Yap, G. P. A.; Crutchley, R. J. *Inorg. Chem.* **2001**, *40*, 1189. (c) Duati, M.; Tasca, S.; Lynch, F. C.; Bohlen, H.; Vos, J. G.; Stagni, S.; Ward, M. D. *Inorg. Chem.* **2003**, *42*, 8377.

(7) (a) Bonvoisin, J. J.; Fabre, M. *J. Am. Chem. Soc.* **2007**, *129*, 1434. (b) Fabre, M.; Jaud, J.; Bonvoisin, J. J. *Inorg. Chim. Acta* **2005**, *358*, 2384. (c) Fabre, M.; Jaud, J.; Hliwa, M.; Launay, J.-P.; Bonvoisin, J. *Inorg. Chem.* **2006**, *45*, 9332.

(8) (a) Albrecht, M. *Chem. Rev.* **2010**, *110*, 576. (b) Djukic, J.-P.; Sortais, J.-B.; Barloy, L.; Pfeffer, M. *Eur. J. Inorg. Chem.* **2009**, 817.

(9) Coudret, C.; Fraysse, S.; Launay, J.-P. *Chem. Commun.* **1998**, 663.

(10) Yang, W.-W.; Wang, L.; Zhong, Y.-W.; Yao, J. *Organometallics* **2011**, *30*, 2236.

(11) (a) Yang, W.-W.; Zhong, Y.-W.; Yoshikawa, S.; Shao, J.-Y.; Masaoka, S.; Sakai, K.; Yao, J.; Haga, M.-a. *Inorg. Chem.* **2012**, *51*, 890. (b) Concepcion, J. J.; Tsai, M.-K.; Muckerman, J. T.; Meyer, T. J. *J. Am. Chem. Soc.* **2010**, *132*, 1545.

(12) (a) Beley, M.; Collin, J.-P.; Louis, R.; Metz, B.; Sauvage, J.-P. *J. Am. Chem. Soc.* **1991**, *113*, 8522. (b) Patoux, C.; Launay, J.-P.; Beley, M.; Chodorowski-Kimmers, S.; Collin, J.-P.; James, S.; Sauvage, J.-P. *J. Am. Chem. Soc.* **1998**, *120*, 3717.

(13) (a) Fraysse, S.; Coudret, C.; Launay, J.-P. *J. Am. Chem. Soc.* **2003**, *125*, 5880. (b) Gao, L.-B.; Kan, J.; Fan, Y.; Zhang, L.-Y.; Liu, S.-H.; Chen, Z.-N. *Inorg. Chem.* **2007**, *46*, 5651. (c) Vilà, N.; Zhong, Y.-W.; Henderson, J. C.; Abruña, H. D. *Inorg. Chem.* **2010**, *49*, 796. (d) Yao, C.-J.; Sui, L.-Z.; Xie, H.-Y.; Xiao, W.-J.; Zhong, Y.-W.; Yao, J. *Inorg. Chem.* **2010**, *49*, 8347. (e) Yao, C.-J.; Zhong, Y.-W.; Yao, J. *J. Am. Chem. Soc.* **2011**, *133*, 15697. (f) Sui, L.-Z.; Yang, W.-W.; Yao, C.-J.; Xie, H.-Y.; Zhong, Y.-W. *Inorg. Chem.* **2012**, *51*, 1590.

(14) (a) Wang, L.; Yang, W.-W.; Zheng, R.-H.; Shi, Q.; Zhong, Y.-W.; Yao, J. *Inorg. Chem.* **2011**, *50*, 7074. (b) Yang, W.-W.; Yao, J.; Zhong, Y.-W. *Organometallics* **2012**, *31*, 1035.

(15) (a) Sutter, J.-P.; Grove, D. M.; Beley, M.; Collin, J.-P.; Veldman, N.; Spek, A. L.; Sauvage, J.-P.; van Koten, G. *Angew. Chem., Int. Ed.* **1994**, *33*, 1282. (b) Steenwinkel, P.; Grove, D. M.; Veldman, N.; Spek, A. L.; van Koten, G. *Organometallics* **1998**, *17*, 5647.

(16) Gagliardo, M.; Amijs, C. H. M.; Lutz, M.; Spek, A. L.; Havenith, R. W. A.; Hartl, F.; van Klink, G. P. M.; van Koten, G. *Inorg. Chem.* **2007**, *46*, 11133.

(17) (a) Haga, M.-a.; Takasugi, T.; Tomie, A.; Ishizuya, M.; Yamada, T.; Hossain, M. D.; Inoue, M. *Dalton Trans.* **2003**, 2069. (b) Haga, M.-a.; Ali, M. M.; Koseki, S.; Fujimoto, K.; Yoshimura, A.; Nozaki, K.; Ohno, T.; Nakajima, K.; Stufkens, D. J. *Inorg. Chem.* **1996**, *35*, 3335.

(18) (a) D'Alessandro, D. M.; Keene, F. R. *Dalton Trans.* **2004**, 3950. (b) Evans, D. H. *Chem. Rev.* **2008**, *108*, 2113. (c) Geiger, W. E.; Barrière, F. *Acc. Chem. Res.* **2010**, *43*, 1030.

(19) (a) Hush, N. S. *Prog. Inorg. Chem.* **1967**, *8*, 391. (b) Hush, N. S. *Electrochim. Acta* **1968**, 1005.

(20) Brunschwig, B. S.; Creutz, C.; Sutin, N. *Chem. Soc. Rev.* **2002**, *31*, 168.

(21) Hush, N. S. *Coord. Chem. Rev.* **1985**, *64*, 135.

(22) (a) Glover, S. D.; Kubiak, C. P. *J. Am. Chem. Soc.* **2011**, *133*, 8721. (b) Londergan, C. H.; Rocha, R. C.; Brown, M. G.; Shreve, A. P.; Kubiak, C. P. *J. Am. Chem. Soc.* **2003**, *125*, 13912.
(23) (a) Sodupe, M.; Bertran, J.; Rodriguez-Santiago, L.; Baerends, E. J. *J. Phys. Chem. A* **1999**, *103*, 166. (b) Gruning, M.; Gritsenko, O. V.; van Gisbergen, S. J. A.; Baerends, E. J. *J. Phys. Chem. A* **2001**, *105*, 9211.
(24) (a) Evans, C. E. B.; Naklicki, M. L.; Rezvani, A. R.; White, C. A.; Kondratiev, V. V.; Crutchley, R. J. *J. Am. Chem. Soc.* **1998**, *120*, 13096. (b) Cruetz, C.; Newton, M. D.; Sutin, N. *J. Photochem. Photobiol. A: Chem.* **1994**, *82*, 47. (c) Wenger, O. S. *Acc. Chem. Res.* **2011**, *44*, 25.
(25) (a) Yao, C.-J.; Zhong, Y.-W.; Nie, H.-J.; Abruña, H. D.; Yao, J. *J. Am. Chem. Soc.* **2011**, *133*, 20720. (b) Kaim, W. *Coord. Chem. Rev.* **2011**, *255*, 2503. (c) Ward, M. D. *J. Solid State Electrochem.* **2005**, *9*, 778.
(26) (a) Wadman, S. H.; Kroom, J. M.; Bakker, K.; Lutz, M.; Spek, A. L.; van Klink, G. P. M.; van Koten, G. *Chem. Commun.* **2007**, 1907. (b) Nemykin, V. N.; Rohde, G. T.; Barrett, C. D.; Hadt, R. G.; Bizzarri, C.; Galloni, P.; Floris, B.; Nowik, I.; Herber, R. H.; Marrani, A. G.; Zanoni, R.; Loim, N. M. *J. Am. Chem. Soc.* **2009**, *131*, 14969. (c) Robson, K. C. D.; Koivisto, B. D.; Yella, A.; Sporinova, B.; Nazeeruddin, M. K.; Baumgartner, T.; Gratzel, M.; Berlinguette, C. P. *Inorg. Chem.* **2011**, *50*, 5494. (d) Bomben, P. G.; Gordon, T. J.; Schott, E.; Berlinguette, C. P. *Angew. Chem., Int. Ed.* **2011**, *50*, 10682.
(27) (a) Becke, A. D. *J. Chem. Phys.* **1993**, *98*, 5648. (b) Lee, C.; Yang, W.; Parr, R. G. *Phys. Rev. B* **1988**, *37*, 785.
(28) Frisch, M. J.; Trucks, G. W.; Schlegel, H. B.; Scuseria, G. E.; Robb, M. A.; Cheeseman, J. R.; Montgomery, J. A., Jr.; Vreven, T.; Kudin, K. N.; Burant, J. C.; Millam, J. M.; Iyengar, S. S.; Tomasi, J.; Barone, V.; Mennucci, B.; Cossi, M.; Scalmani, G.; Rega, N.; Petersson, G. A.; Nakatsuji, H.; Hada, M.; Ehara, M.; Toyota, K.; Fukuda, R.; Hasegawa, J.; Ishida, M.; Nakajima, T.; Honda, Y.; Kitao, O.; Nakai, H.; Klene, M.; Li, X.; Knox, J. E.; Hratchian, H. P.; Cross, J. B.; Adamo, C.; Jaramillo, J.; Gomperts, R.; Stratmann, R. E.; Yazyev, O.; Austin, A. J.; Cammi, R.; Pomelli, C.; Ochterski, J. W.; Ayala, P. Y.; Morokuma, K.; Voth, G. A.; Salvador, P.; Dannenberg, J. J.; Zakrzewski, V. G.; Dapprich, S.; Daniels, A. D.; Strain, M. C.; Farkas, O.; Malick, D. K.; Rabuck, A. D.; Raghavachari, K.; Foresman, J. B.; Ortiz, J. V.; Cui, Q.; Baboul, A. G.; Clifford, S.; Cioslowski, J.; Stefanov, B. B.; Liu, G.; Liashenko, A.; Piskorz, P.; Komaromi, I.; Martin, R. L.; Fox, D. J.; Keith, T.; Al-Laham, M. A.; Peng, C. Y.; Nanayakkara, A.; Challacombe, M.; Gill, P. M. W.; Johnson, B.; Chen, W.; Wong, M. W.; Gonzalez, C.; Pople, J. A. *Gaussian 03*, revision E.01; Gaussian Inc.: Pittsburgh, PA, 2007.
(29) (a) Hay, P. J.; Wadt, W. R. *J. Chem. Phys.* **1985**, *82*, 270. (b) Wadt, W. R.; Hay, P. J. *J. Chem. Phys.* **1985**, *82*, 284. (c) Hay, P. J.; Wadt, W. R. *J. Chem. Phys.* **1985**, *82*, 299.
(30) (a) Dunning, T. H.; Hay, P. J. In *Modern Theoretical Chemistry*; Schaefer, H. F., Ed.; Plenum: New York, 1976; Vol. 3, p 1. (b) Hehre, W. J.; Radom, L.; Schleyer, P. V. R.; Pople, J. A. *Ab Initio Molecular Orbital Theory*; John Wiley & Sons: New York, 1986.
(31) (a) Klamt, A.; Schüürmann, G. *J. Chem. Soc., Perkin Trans. 2* **1993**, 799. (b) Andzelm, J.; Kölmel, C.; Klamt, A. *J. Chem. Phys.* **1995**, *103*, 9312. (c) Barone, V.; Cossi, M. *J. Phys. Chem. A* **1998**, *102*, 1995. (d) Cossi, M.; Rega, N.; Scalmani, G.; Barone, V. *J. Comput. Chem.* **2003**, *24*, 669.